



# Binding of *Staphylococcus aureus* Protein A to von Willebrand Factor Is Regulated by Mechanical Force

Felipe Viela,<sup>a</sup> Valeria Prystopiuk,<sup>a</sup> Audrey Leprince,<sup>b</sup> Jacques Mahillon,<sup>b</sup> Pietro Speziale,<sup>c,d</sup> Giampiero Pietrocola,<sup>c</sup> Yves F. Dufrêne<sup>a,e</sup>

<sup>a</sup>Institute of Life Sciences, Université Catholique de Louvain, Louvain-la-Neuve, Belgium

<sup>b</sup>Laboratory of Food and Environmental Microbiology, Earth and Life Institute, Université Catholique de Louvain, Louvain-la-Neuve, Belgium

<sup>c</sup>Department of Molecular Medicine, Unit of Biochemistry, University of Pavia, Pavia, Italy

<sup>d</sup>Department of Industrial and Information Engineering, University of Pavia, Pavia, Italy

<sup>e</sup>Walloon Excellence in Life sciences and Biotechnology (WELBIO), Liege, Belgium

**ABSTRACT** Binding of *Staphylococcus aureus* to the large plasma glycoprotein von Willebrand factor (vWF) is controlled by hydrodynamic flow conditions. Currently, we know little about the molecular details of this shear-stress-dependent interaction. Using single-molecule atomic force microscopy, we demonstrate that vWF binds to the *S. aureus* surface protein A (SpA) via a previously undescribed force-sensitive mechanism. We identify an extremely strong SpA-vWF interaction, capable of withstanding forces of  $\sim 2$  nN, both in laboratory and in clinically relevant methicillin-resistant *S. aureus* (MRSA) strains. Strong bonds are activated by mechanical stress, consistent with flow experiments revealing that bacteria adhere in larger amounts to vWF surfaces when the shear rate is increased. We suggest that force-enhanced adhesion may involve conformational changes in vWF. Under force, elongation of vWF may lead to the exposure of a high-affinity cryptic SpA-binding site to which bacteria firmly attach. In addition, force-induced structural changes in the SpA domains may also promote strong, high-affinity binding. This force-regulated interaction might be of medical importance as it may play a role in bacterial adherence to platelets and to damaged blood vessels.

**IMPORTANCE** *Staphylococcus aureus* protein A (SpA) binds to von Willebrand factor (vWF) under flow. While vWF binding to SpA plays a role in *S. aureus* adherence to platelets and endothelial cells under shear stress, the molecular basis of this stress-dependent interaction has not yet been elucidated. Here we show that the SpA-vWF interaction is regulated by a new force-dependent mechanism. The results suggest that mechanical extension of vWF may lead to the exposure of a high-affinity cryptic SpA-binding site, consistent with the shear force-controlled functions of vWF. Moreover, strong binding may be promoted by force-induced structural changes in the SpA domains. This study highlights the role of mechanoregulation in controlling the adhesion of *S. aureus* and shows promise for the design of small inhibitors capable of blocking colonization under high shear stress.

**KEYWORDS** adhesion, *Staphylococcus aureus*, atomic force microscopy, mechanical force, von Willebrand factor

*Staphylococcus aureus* is a leading cause of endovascular infections, such as infective endocarditis or heart valve prosthetic infection (1, 2). During endovascular infections, the pathogen needs to attach to the endothelium and to withstand the shear stress of flowing blood. *S. aureus* binds to endothelium under flow via von Willebrand factor (vWF) (3–5), a large multimeric glycoprotein produced by endothelial cell layers and stored in Weibel-Palade bodies and  $\alpha$ -granules of platelets. The basic vWF mono-

**Citation** Viela F, Prystopiuk V, Leprince A, Mahillon J, Speziale P, Pietrocola G, Dufrêne YF. 2019. Binding of *Staphylococcus aureus* protein A to von Willebrand factor is regulated by mechanical force. *mBio* 10:e00555-19. <https://doi.org/10.1128/mBio.00555-19>.

**Invited Editor** Gerard Lina, Centre International de Recherche en Infectiologie

**Editor** Gerald B. Pier, Harvard Medical School

**Copyright** © 2019 Viela et al. This is an open-access article distributed under the terms of the [Creative Commons Attribution 4.0 International license](https://creativecommons.org/licenses/by/4.0/).

Address correspondence to Giampiero Pietrocola, [giampiero.pietrocola@unipv.it](mailto:giampiero.pietrocola@unipv.it), or Yves F. Dufrêne, [yves.dufrene@uclouvain.be](mailto:yves.dufrene@uclouvain.be).

**Received** 28 February 2019

**Accepted** 29 March 2019

**Published** 30 April 2019

mer is a 2,050-amino-acid protein containing four types of repeat domains, A, B, C, and D, which are arranged in the sequence D1-D2-D'-D3-A1-A2-A3-D4-B1-B2-B3-C1-C2-CK in the mature protein. vWF is a multifunctional protein interacting with a variety of ligands. The D'/D3 domain binds factor VIII, the A1 domain binds to platelet GPIb receptor, heparin, and possibly collagen, the A2 domain contains the buried cleavage site for the specific ADAM13 protease, the A3 domain binds collagen, and the C1 domain contains an RGD motif involved in binding platelet integrin  $\alpha$ IIb $\beta$ 3. After secretion, vWF is elongated as a result of blood flow and forms fibers on endothelial layers. In contrast to the globular state, vWF under shear exposes cryptic glycoprotein platelet binding sites to which platelets bind with high affinity. The transition from a compact into an extended conformation leads to the activation of the vWF A1 domain to bind platelets (6).

*S. aureus* interacts with vWF using the bacterial cell surface protein A (SpA) (7, 8), the secreted coagulase Willebrand factor-binding protein (vWFbp) (8, 9), and clumping factor A (ClfA) (5). SpA is a 55-kDa protein (which including the signal peptide, may differ between isolates) comprising five N-terminal tandemly linked triple-helical bundle domains, each of which binds to different ligands, including the IgG Fc region, the tumor necrosis factor receptor 1 (TNFR-1) (10), and the epidermal growth factor receptor (EGFR) (11), followed by the repeat containing the Xr and the nonrepetitive Xc regions. SpA also binds with high affinity to the vWF A1 domain and to a lesser extent to the D'/D3 domains (12).

There is increasing evidence that binding of vWF to *S. aureus* is controlled by hydrodynamic flow. Under fluid shear stress, ClfA binds via vWFbp to vWF present on activated endothelial cells (4, 5). In addition, ClfA binds in a shear-dependent manner to fibrinogen, which, in turn, interacts with integrins expressed by endothelial cells, suggesting a dual role of the adhesin in *S. aureus* adhesion to endothelium (13). Shear flow has also been shown to increase SpA-dependent bacterial attachment to endothelial cell monolayers and to the extracellular matrix (3, 8, 12). While these flow experiments show that *S. aureus*-vWF adhesion is modulated by shear stress, the underlying molecular mechanisms are poorly understood. Here we unravel the strength and dynamics of the SpA-vWF interaction using single-molecule atomic force microscopy (AFM) (14). We find that SpA mediates *S. aureus* adhesion to vWF via a novel force-dependent mechanism involving conformational changes in the vWF and SpA molecules. The stress-induced activation of the SpA-vWF interaction may be critical for bacterial adherence to platelets and to damaged blood vessels.

## RESULTS

**SpA favors bacterial adhesion to vWF, both *in vitro* and on endothelial cells.** To confirm the role of SpA in promoting bacterial adhesion to vWF, we studied the attachment of the *S. aureus* Newman strain, known to largely express SpA (15–17), onto vWF immobilized on microtiter wells. Wild-type (WT) bacteria adhered to vWF in large amounts, whereas bacteria from the Newman  $\Delta$ *spa* strain lacking the adhesin did to a much lower extent (Fig. 1A). Adhesion of WT bacteria was inhibited by soluble SpA, demonstrating the specificity of interaction (Fig. 1A). Optical microscopy imaging confirmed that SpA is involved in vWF-dependent adhesion since WT bacteria, unlike  $\Delta$ *spa* ones, extensively colonized vWF-covered glass substrates (Fig. 1B). Note that this optical assay confirms proper expression of SpA, but should not be considered quantitative as some shear stress was applied during rinsing.

We also investigated bacterial adhesion to vWF in the extracellular matrix (ECM) of human umbilical vein endothelial cells (HUVECs). To promote vWF exposure, endothelial cells were allowed to spread on glass surfaces and then treated with the calcium ionophore A23187. Upon ionophore activation, the Weibel-Palade bodies are transported to the cell surface, releasing vWF, which is temporarily retained on the cell surface, thus making it available for interaction with *S. aureus* (18). Incubating monolayers with a specific vWF antibody, we found that the vWF release increased with the concentration of ionophore added (Fig. 1C). In line with this, confocal microscopy

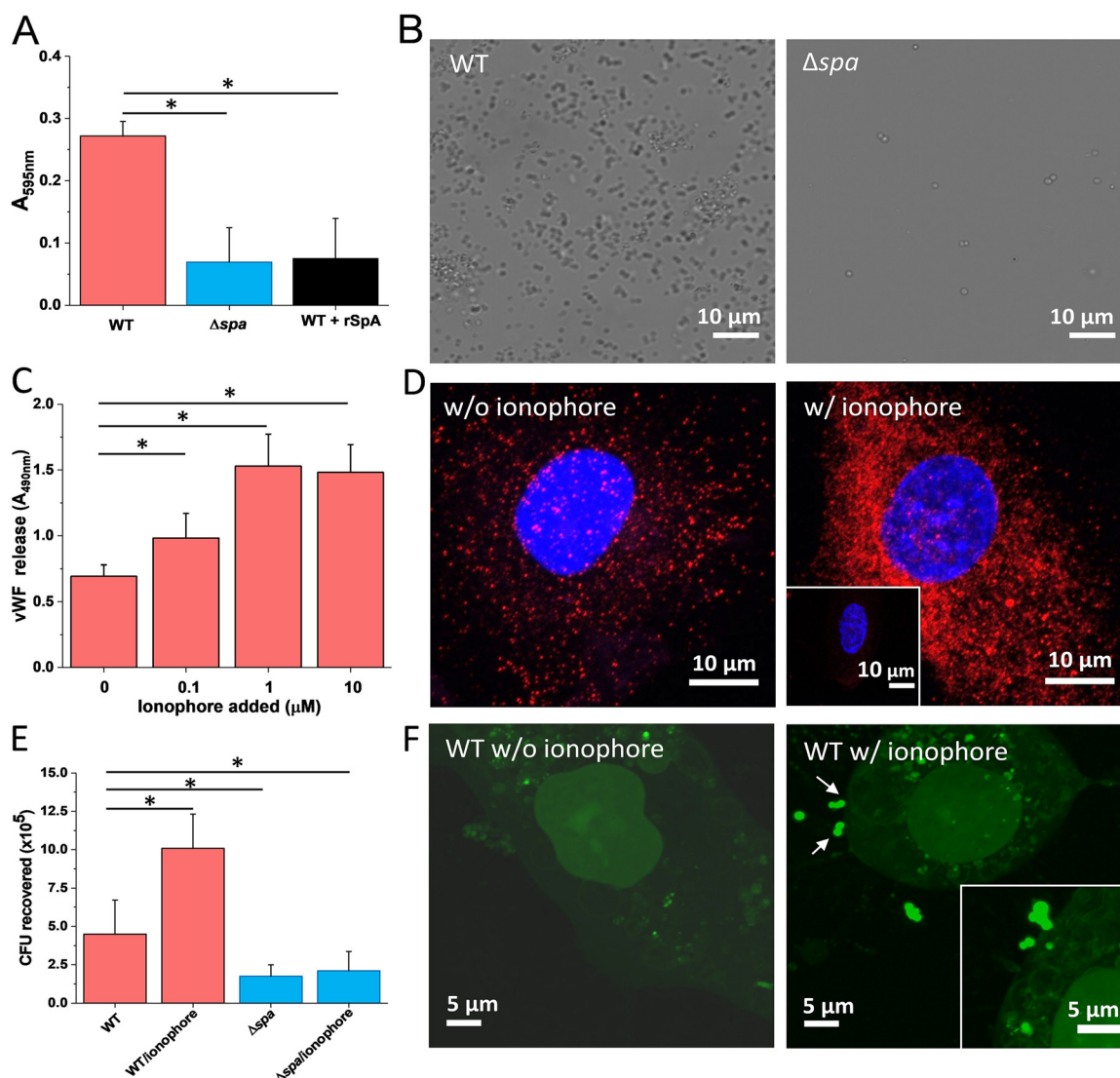


**FIG 1** Attachment of *S. aureus* to immobilized vWF and to endothelial cells. (A) Microtiter wells coated with vWF were incubated with *S. aureus* Newman WT and Newman  $\Delta spa$  bacteria, rinsed, and stained with crystal violet, and the absorbance at 595 nm was measured in an ELISA plate reader. Attachment of WT bacteria was also performed in the presence of 2  $\mu g$  soluble SpA. (B) Optical microscopy images of *S. aureus* Newman WT and Newman  $\Delta spa$  bacteria adhering to vWF-coated substrates. (C) vWF release by endothelial cells. Confluent HUVEC monolayers were incubated with increasing concentrations of calcium ionophore A23187 for 10 min. The vWF released in the extracellular matrix was determined with rabbit anti-vWF polyclonal antibody followed by HRP-conjugated goat anti-rabbit. (D) Imaging of vWF release. Shown are confocal microscopy images of HUVECs before (left) and after (right) treatment with calcium ionophore. Staining with mouse anti-vWF antibody and secondary goat anti-mouse Alexa Fluor 647 antibody documents the release of large amounts of vWF upon ionophore treatment (vWF is in red, and the nucleus is in blue). The inset shows a control experiment in which the primary antibody was missing. (E) Endothelial cell adhesion assays. Confluent HUVECs were incubated with *S. aureus* Newman WT and Newman  $\Delta spa$  bacteria for 90 min, in the presence or absence of 1  $\mu M$  ionophore. The number of adhering bacteria was determined as described in Materials and Methods. (F) Imaging of bacterial-endothelial cell adhesion. Confluent HUVECs, treated (right) or not (left) with ionophore, were incubated with *S. aureus* Newman WT bacteria stained with the BacLight viability kit, rinsed, and imaged by confocal microscopy. The arrows indicate bacteria adhering to the endothelial cell surface. For all plots, means and SD of results from two independent experiments, each performed in triplicate, are presented. Statistically significant difference is indicated (Student's *t* test; \*,  $P < 0.05$ ).

revealed that treatment with the ionophore largely increased the exposure of vWF in the ECM (Fig. 1D). Microscopic adhesion assays showed that WT bacteria attached in much larger amounts to HUVECs when these were activated with ionophore (Fig. 1E and F). The  $\Delta spa$  strain showed much lower adhesion than the WT, both with and without ionophore. Some residual attachment was observed, suggesting that other adhesins may play a role. The above observations show that, under our conditions, *S. aureus* binds to vWF both *in vitro* and on endothelial cells primarily via SpA proteins.

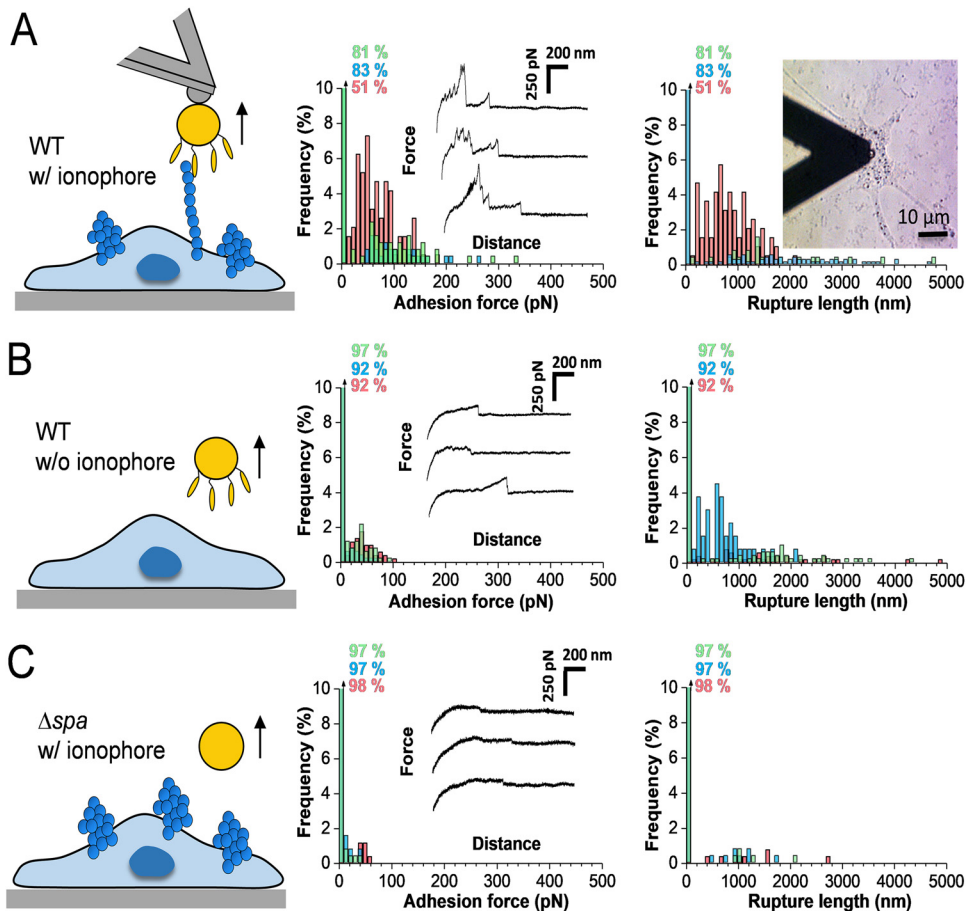


**FIG 2** Adhesion forces between *S. aureus* and vWF in the extracellular matrix. (A) Maximum adhesion force (left) and rupture length (right) histograms with representative retraction force profiles (insets) obtained by recording force-distance curves in HEPES buffer between Newman bacteria and ionophore-treated endothelial cells. Data from a total of 1,536 curves from 3 different bacterial-HUVEC cell pairs are shown. (B) Force data collected between Newman bacteria and nontreated endothelial cells (1,536 curves from 3 cell pairs). (C) Force data collected between Newman  $\Delta spa$  bacteria and ionophore-treated endothelial cells (1,536 curves from 3 cell pairs). The percentage shown represents the proportion of nonadhesive events. For data on more cells, see Table S1.

The low adhesion of the  $\Delta spa$  strain is in contrast with the results of Claes et al. (4, 5) showing that under high fluid shear stress, ClfA binds via vWfbp to vWF on activated endothelial cells. However, our adhesion assays were not performed at high stress. It is also possible that under our conditions, bacteria did not secrete much vWfbp proteins as the cells were centrifuged before used. Additionally, the involvement of vWfbp could vary, depending on the secreted amount of vWfbp, its rebinding to ClfA, and the availability of surface-expressed ClfA to interact with this protein.

**Adhesion forces between single *S. aureus* bacteria and vWF.** We measured the interaction forces between *S. aureus* and vWF in the ECM of HUVECs using AFM (Fig. 2). Shown in Fig. 2A are the adhesion forces, rupture lengths, and representative force curves obtained between single Newman bacteria and ionophore-treated endothelial cells (3 representative bacterial-HUVEC cell pairs [for more data, see Table S1 in the supplemental material]). Force curves ( $27\% \pm 18\%$ ) showed multiple adhesion peaks of a magnitude of  $114 \pm 55$  pN (mean  $\pm$  standard deviation [SD];  $n = 684$  adhesive curves from 10 cell pairs [Table S1]) and  $1,679 \pm 974$ -nm rupture lengths ( $n = 684$ ). Much weaker adhesion was observed with native, untreated endothelial cells (Fig. 2B; Table S1), or when using the Newman  $\Delta spa$  mutant (Fig. 2C; Table S1), demonstrating that the  $\sim 100$ -pN forces are associated with specific SpA-vWF bonds. The shape of adhesive curves did not change over time, indicating that the bacterial cell probes were not

denatured or contaminated during repeated force curve measurements. Force profiles did not show force plateaus, meaning membrane tethers were not formed upon pulling. This indicates that bacteria did not directly interact with the endothelial cell membrane, but rather with loosely anchored vWF. As the vWF-ECM interaction is probably the weak side of the three-component complex, under force, the vWF-ECM bond will rupture before the SpA-vWF bond.

To unravel the strength of the SpA-vWF interaction, we therefore analyzed the forces between *S. aureus* and vWF immobilized on solid substrates. As shown in Fig. 3A, force profiles between single Newman bacteria and vWF featured strong adhesion peaks with mean forces of  $2,116 \pm 235$  pN (mean  $\pm$  SD;  $n = 659$  adhesive curves from 3 cells [for more cells, see Fig. S1A in the supplemental material]) and mean rupture length of  $213 \pm 92$  nm ( $n = 659$ ). These forces are specific to the SpA-vWF interaction as they were lacking in Newman  $\Delta spa$  cells (Fig. 3B). High forces reflect the rupture of single bonds rather than multiple weak bonds as such sharp force distributions were observed in multiple cells, as well as in single-molecule experiments with vWF-coated AFM tips (Fig. 4 [see below]). The bonds ruptured at  $\sim 200$  to  $300$  nm, which is in the range of the length of the unfolded SpA protein ( $\sim 180$  nm, assuming the adhesin is made of  $\sim 500$  residues [19]). However, it is likely that vWF will also contribute to protein extensions (see below), meaning that SpA would not be completely unfolded.

Are the interaction forces observed on the Newman laboratory strain clinically relevant? We found that cells from the methicillin-resistant *S. aureus* (MRSA) LAC\* strain, a member of the USA300 lineage and a strong producer of SpA, featured strong adhesion signatures similar to those of the Newman strain (Fig. 3C; Fig. S1B). Adhesion forces were strongly reduced in LAC\*  $\Delta spa$  mutant cells deficient in SpA (Fig. 3D), implying again they involve SpA proteins. Rupture lengths were larger than with Newman cells ( $\sim 300$  nm and sometimes even longer), implying that not only SpA but also vWF was elongated upon pulling. Thus, the strong vWF-binding forces measured in the laboratory strain also apply to the clinically relevant strain.

**Mechanical strength of the SpA-vWF complex.** To dissect the mechanical strength of the SpA-vWF complex, Newman cells were probed using single-molecule AFM with vWF-modified tips (Fig. 4A; 3 different cells [for more cells, see Fig. S2 in the supplemental material]). About 15% of the force curves featured adhesion events with a small number of weak adhesion peaks of  $107 \pm 56$  pN and a large fraction of strong peaks of  $2,313 \pm 217$  pN ( $n = 458$  adhesive curves from 3 cells). Most adhesion events were abolished with Newman  $\Delta spa$  cells (Fig. 4B), supporting the specificity of the measurements. Mostly single bonds were probed because strong forces showed a narrow distribution and featured single rupture peaks, which is not expected if the number of bonds varied from one pull to another. Rupture lengths featured a more complex pattern than with whole cells (Fig. 3), with values ranging from  $\sim 100$  to  $400$  nm. The extent to which SpA is unfolded upon pulling is not known. However, as the length of the fully unfolded SpA is  $\sim 180$  nm (assuming the adhesin is made of  $\sim 500$  residues [19]), our values show that vWF contributes to protein extensions. We therefore suggest that the  $\sim 100$ - to  $200$ -nm and  $\sim 200$ - to  $400$ -nm ruptures may result from a change in the structure of vWF, from a globular state to an extended chain conformation. Single-molecule imaging suggested that the adhesins form clusters on the cell surface (Fig. 4A to C, insets), a phenomenon that could enhance bacterial adhesion through multivalency.

**Mechanoregulation of the SpA-vWF bond.** As vWF binding to *S. aureus* is influenced by shear stress conditions, we hypothesized that the strength of the SpA-vWF bond might depend on mechanical force. Figure 5A shows the SpA-vWF adhesion force ( $F$ ) measured on Newman bacteria with vWF-modified tips while varying the loading rate ( $LR$ ; assessed from force versus time curves [20, 21]) (data pooled from 2,468 adhesive peaks from 6 cells). Two clouds of data points corresponding to low and high forces can be distinguished. Analysis of the forces over discrete ranges of  $LR$ s (Fig. 5B) revealed that the probability of forming strong bonds increases with the  $LR$ . At low  $LR$ s,

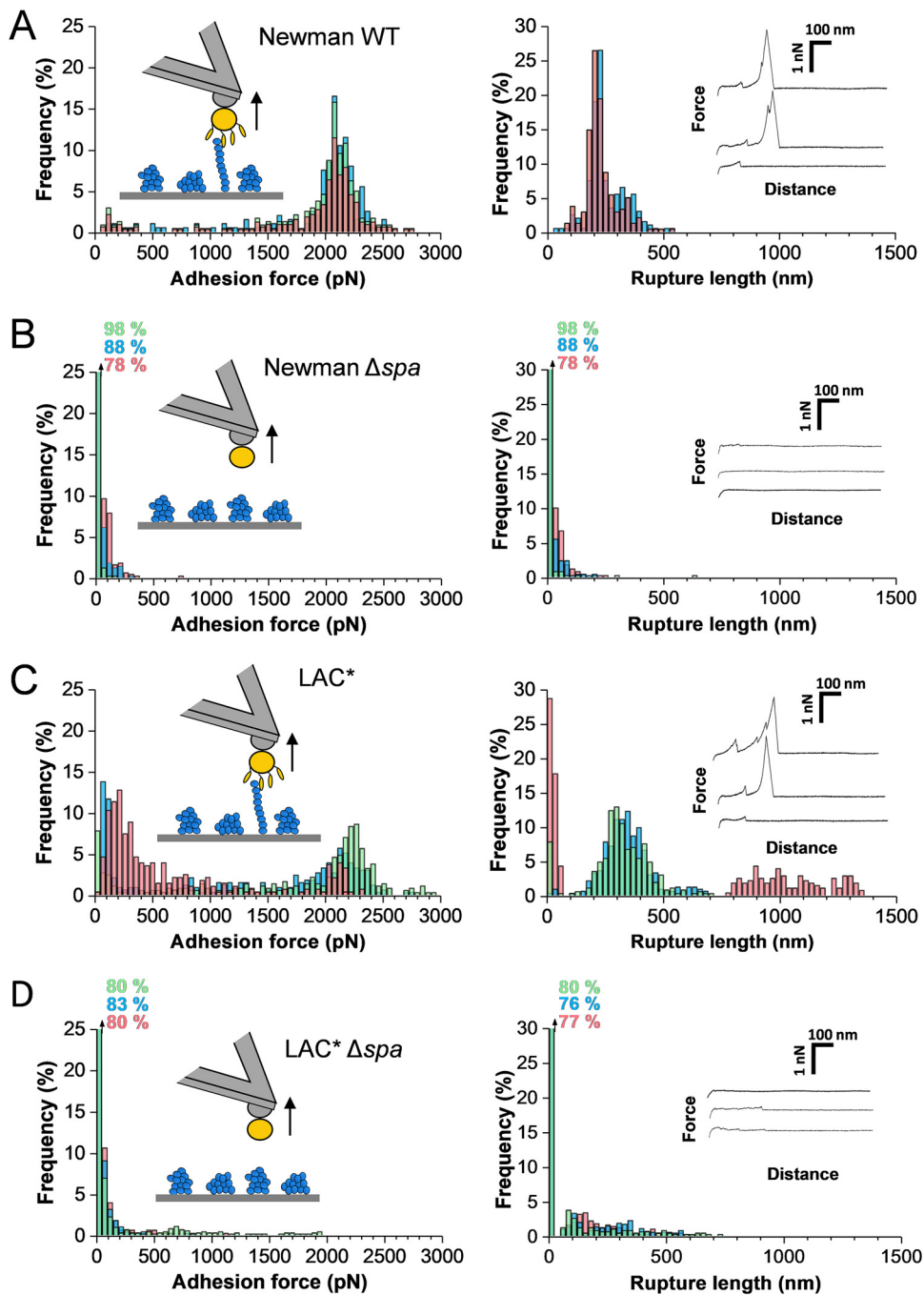


**FIG 3** Adhesion forces between *S. aureus* and immobilized vWF. (A and B) Maximum adhesion force (left) and rupture length (right) histograms with representative retraction force profiles obtained by recording force distance curves in PBS between Newman WT (A) or Newman  $\Delta spa$  (B) bacteria and vWF-coated substrates. (C and D) Force data obtained for the clinically relevant LAC\* strain (C) and its LAC\*  $\Delta spa$  mutant (D). For each panel, data from three representative bacterial cells are shown.

forces of  $146 \pm 68$  pN were seen, while at high LR, forces of  $2,359 \pm 174$  pN dominated. Intermediate forces in the range of 500 to 1,500 pN were never observed. This shift in force distribution demonstrates that the SpA-vWF interaction strengthens under mechanical tension.

We also estimated the mechanical stiffness ( $k_m$ ) of the SpA-vWF molecular complex under low and high tension (Fig. 5C), using the slope ( $s$ ) of the linear portion of the raw deflection versus piezo displacement curves and the following equation:  $k_m = (k_c \times s) /$

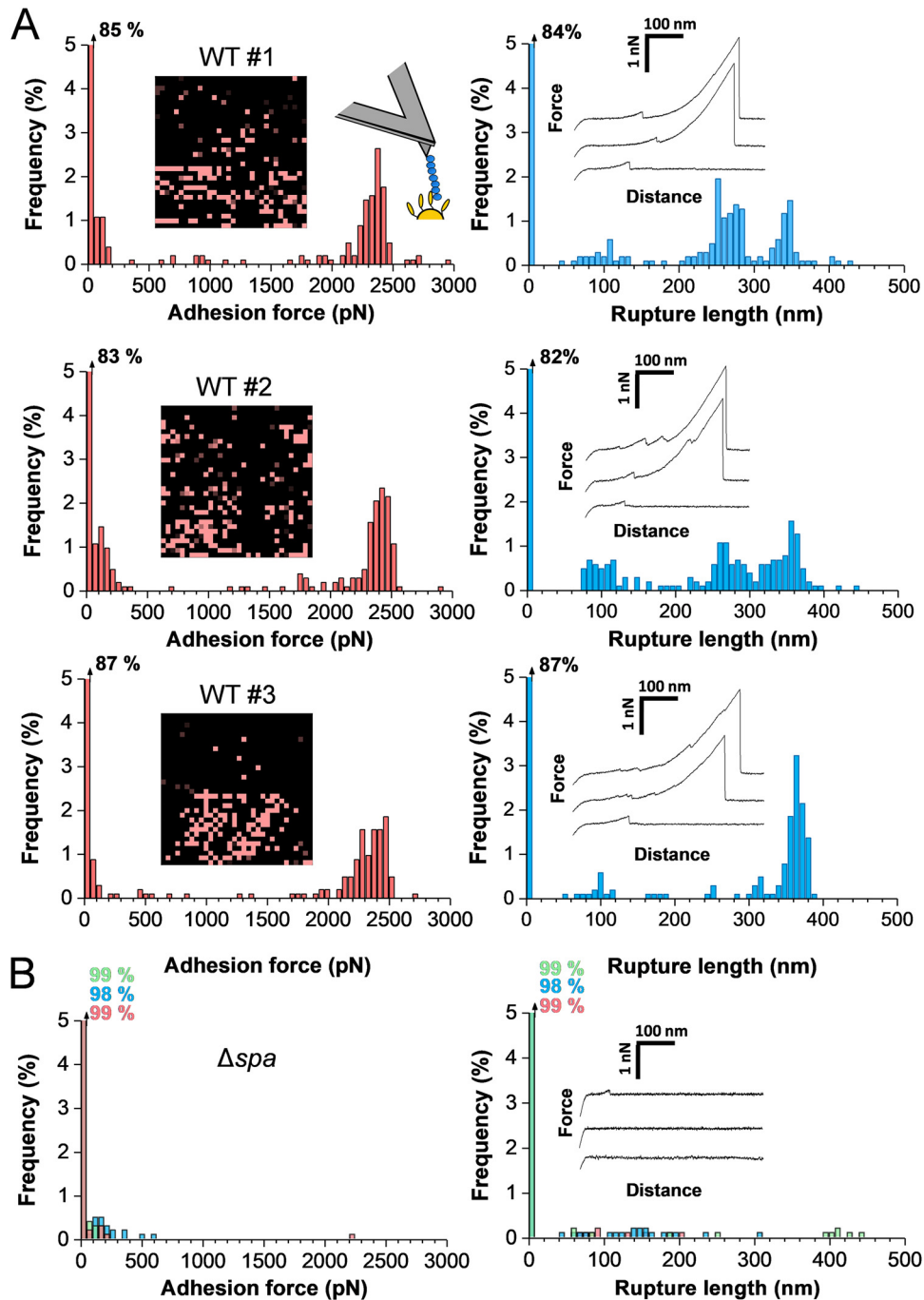


**FIG 4** Strength of single SpA-vWF bonds. (A) Maximum adhesion force histograms (left) with force maps (insets; image size = 500 nm) and rupture length histograms (right) with representative retraction force profiles (insets) obtained by recording force-distance curves in PBS between 3 different Newman WT bacteria and vWF-modified AFM tips. (B) Data obtained under the same conditions for Newman  $\Delta spa$  bacteria. (Data from 3 cells are merged.)

( $1 - s$ ), where  $k_c$  is the spring constant of the AFM cantilever (21). Weak and strong forces featured values of  $k_m = 4.2 \pm 0.2$  pN nm<sup>-1</sup> and  $k_m = 24 \pm 5$  pN nm<sup>-1</sup>, respectively, revealing that the strength and stiffness of the bonds were correlated. This was also evident by plotting the stiffness versus adhesion force of the complex for all force curves (Fig. 5D). These observations suggest that mechanical force induces a structural change in the complex, from a folded, weakly binding state to an extended, strongly binding state.

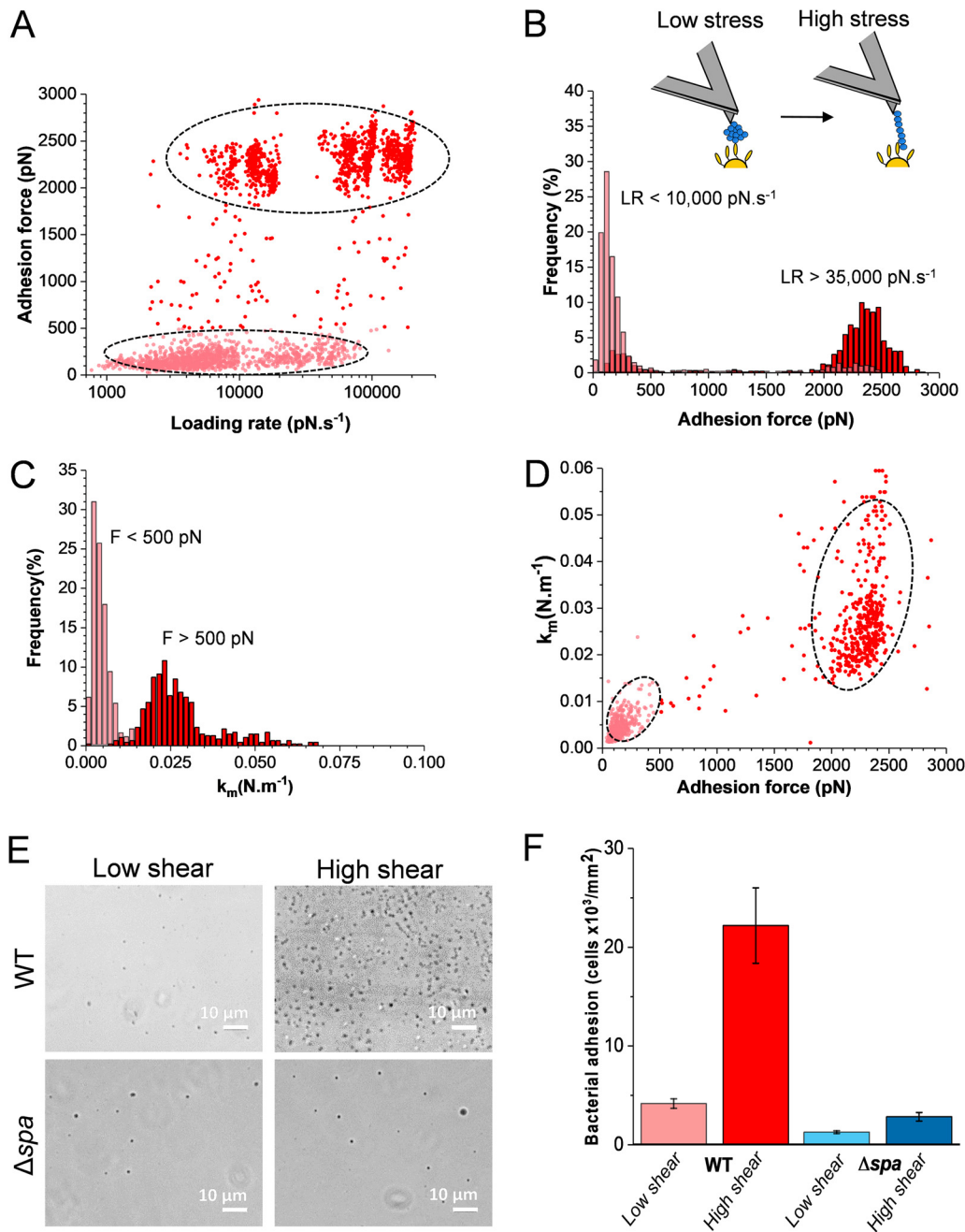


**FIG 5** Mechanical activation of vWF binding to SpA. (A) Strength of single SpA-vWF bonds measured at increasing loading rates (LRs) on Newman WT bacteria (2,468 adhesive events from 6 cells). All adhesion peaks were analyzed to take into account all possible interactions. (B) Analysis of the data in panel A showing that strong bonds are favored at high LR. Discrete ranges of LRs were binned, and the forces were plotted as histograms (see Fig. S3 in the supplemental material). (C) Stiffness of the SpA-vWF complex ( $k_m$ ) at low (<500 pN) and high (>500 pN) tensile forces. A cutoff of 500 pN was chosen as essentially all low adhesion forces at low stress were smaller than this value (see panel B). (D) Plot of  $k_m$  as a function of the adhesion force showing that the high mechanical stability of the bond correlates with a high molecular stiffness. (E and F) SpA-dependent bacterial adhesion to vWF increases with fluid shear stress. Shown are optical microscopy images of Newman WT and  $\Delta spa$  bacteria adhering to vWF-coated surfaces in a microparallel flow chamber under low and high shear stresses. Shown in panel F is the quantification of the amounts of adhering bacteria estimated from the experiments described in panel E from a total of 6 images from 3 experiments for each condition.

Lastly, we wondered whether the force-dependent binding of SpA could favor bacterial adhesion under shear flow conditions, as observed with catch bonds (22). To substantiate this further, bacterial adhesion was studied under flow at low and moderate shear stress (Fig. 5E and F). Bacterial suspensions were flowed over vWF-coated

substrates mounted into a microparallel flow chamber, and adhering bacteria were directly observed by optical microscopy. While WT bacteria poorly adhered at low shear rate ( $12 \text{ s}^{-1}$ ), adhesion was largely increased at moderate shear rate ( $120 \text{ s}^{-1}$ ), corresponding to normal venous shear rates (23). Note that there is no clear definition of what are low and high shear rates. In population studies dealing with *S. aureus* adhesion, shear rates of about  $50$  to  $100 \text{ s}^{-1}$  are generally considered low. Therefore, our shear rate of  $120 \text{ s}^{-1}$  should probably be considered moderate rather than high. So while AFM data cover a wide range of shear stresses that are relevant to *in vivo* situations, our flow data only cover a small range of shear stress. Adhesion of  $\Delta spa$  cells was low and independent of shear conditions. This shows that SpA-dependent *S. aureus* adhesion to vWF under fluid flow is increased by shear stress, as reported for the ClfA-mediated adhesion to vWF in flowing blood (4, 5).

## DISCUSSION

How physical stress regulates cellular functions in *S. aureus* is a largely unsolved question. Several studies have shown that SpA-dependent *S. aureus* adhesion to vWF is influenced by fluid shear (12, 24, 25), but the molecular interactions involved have not yet been investigated. Using single-molecule experiments, we have identified a novel mechanism of mechanoregulation of *S. aureus* adhesion in which SpA-vWF bonds are enhanced by mechanical tension. The newly discovered mechanoregulation mechanism reported here might be of medical relevance as it explains how *S. aureus* is capable of resisting high shear forces of flowing blood during endovascular infections and how the pathogen attaches to platelets under fluid shear. In pharmacology, the SpA-vWF bond might be an important target for the development of novel therapeutics against *S. aureus*.

SpA mediates bacterial adhesion to immobilized vWF through specific bonds that are much stronger ( $\sim 2 \text{ nN}$ ) than most receptor-ligand interactions studied to date. Compared to its soluble form, immobilized vWF is biologically important as it promotes platelet adhesion at sites of vascular injury (8). Weaker bonds are detected on endothelial cells, reflecting rupture of vWF weakly anchored in the ECM. Notably, vWF binding to SpA is tightly mechanoregulated: the bond is weak at low tensile force, but is dramatically increased at high force. To understand the molecular origin of the force-dependent SpA-vWF adhesion, it is interesting to compare our results with the forces measured so far for other staphylococcal adhesins, especially the structurally and functionally related *Staphylococcus epidermidis* SdrG and *S. aureus* ClfA and ClfB. The structural features and molecular biology of these three proteins have been widely investigated (26). They bind to their ligands (e.g., fibrinogen) via the well-known dock, lock, and latch (DLL) mechanism. The binding site of these adhesins is a cleft of  $30 \text{ \AA}$  in length between the N2 and N3 subdomains located in the A region of the protein. Once the ligand peptide is docked and stabilized by hydrophobic interactions and hydrogen bonds, a C-terminus extension of the N3 subdomain folds over the ligand to insert and complement a  $\beta$ -sheet in the N2 subdomain. This DLL mechanism thus greatly stabilizes the conformation of the complex (27). Single-molecule AFM experiments have shown that SdrG, ClfA, and ClfB display an extreme mechanical stability (20, 21, 28), with a binding strength much larger than those of all biomolecular bonds studied so far. Recently, the Gaub group used simulations to unravel the mechanism behind this extreme mechanostability (29, 30). They found that the target peptide is confined in a screwlike manner in the binding pocket of SdrG and that the binding strength of the complex results from numerous hydrogen bonds between the peptide backbone and SdrG, independent of peptide side chains. Rupture of the complex requires all hydrogen bonds to be broken simultaneously. Interestingly, ClfA and ClfB may bind their ligands through a catch bond as their binding strength increases as mechanical force is applied (20, 21).

Our findings are novel and unique in that SpA is structurally and functionally very different from SdrG and ClfA/ClfB (26), as well as from other adhesins investigated so far, and does not involve a DLL binding mechanism. The force-regulated SpA-vWF

interaction is likely to involve conformational changes in vWF, and possibly as well in SpA. vWF is a mechanosensitive protein capable of responding to external forces, such as hydrodynamic shear in flowing blood, to tune its biological functions (31). Hydrodynamic forces induce a change in the structure of vWF, from a globular state to an extended chain conformation with exposure of intramolecular globular domains. This stress-induced elongation promotes the adhesion of vWF to platelets and collagen (see, e.g., reference 32). This leads us to suggest that the force-induced extension of vWF may lead to the exposure of cryptic high-affinity binding sites in vWF domains, to which SpA adhesins on the bacterial cell surface strongly bind. The transition from a globular, weak binding state, to a stretched, strong binding state is supported by the long protein extensions that we observed (up to  $\sim 400$  nm versus  $\sim 180$  nm expected for unfolded SpA), implying that vWF is indeed extended under force, and by the correlation between the strength and stiffness of the SpA-vWF complex. In flowing blood, bacteria are exposed to high shear conditions, corresponding to loading rates that can be larger than 100,000 pN/s [33 [see the supplemental material]]. As the SpA-vWF bond is activated at loading rates of 10,000 pN/s, this mechanism will occur *in vivo*. Our model is reminiscent of the binding of the vWF A1 domain to platelet GPIIb $\alpha$ , which is activated through a two-step conformational transition (31): under flow, elongation of vWF from a compact to a linear form leads to the exposure of cryptic binding sites, and then force-induced conformational changes convert the A1 domain from a low-affinity to high-affinity state.

While SpA is not engaged in DLL binding, structural changes in the adhesin may also occur during the force-dependent binding to vWF. SpA includes five small three-helix-bundle domains separated by conserved flexible linkers. The three-dimensional (3D) structure of SpA has only been solved for single domains (34, 35). The relative orientation of successive helical bundles when attached to the bacteria cell has, to our knowledge, not been addressed. Structural studies have revealed that SpA exhibits extensive, unusual multiscale conformational heterogeneity. This structural plasticity could enable SpA to bind multiple partners (34, 35). Analysis of a single domain in complex with an Fc fragment of human IgG shows that structural changes occur in SpA when it binds to Fc, including a significant reduction in conformational heterogeneity as well as displacement of an SpA side chain. These studies suggest that concerted backbone/side-chain changes are used for binding multiple partners. So there might be opportunities for force-induced structural changes in the adhesin domains to favor strong binding to vWF. Clearly, clarification of the molecular nature of the interaction of SpA with vWF requires new structural biology data on the SpA-vWF complex.

## MATERIALS AND METHODS

**Bacterial strains and growth conditions.** We used the laboratory strain Newman and the derivative Newman  $\Delta spa$  mutant deficient in protein A (36). We also studied a MRSA isolate called LAC\*, an erythromycin-sensitive variant of LAC that is a strong producer of SpA (37), and the derivative LAC\*  $\Delta spa$  mutant deficient in protein A (38). All strains were grown in brain heart infusion (BHI) broth with shaking at 200 rpm at 37°C to stationary phase. For AFM experiments, cells were harvested by centrifugation at  $2,500 \times g$  for 5 min and washed twice with phosphate-buffered saline (PBS).

**Cell culture.** Human umbilical vein endothelial cells (HUVECs) from a single donor (Lonza, Spain) were cultured in T25 flasks (Becton, Dickinson, Germany) and incubated at 37°C in 5% CO<sub>2</sub> with 100% humidity. Commercial basal medium, supplemented with growth factors and cytokines (EGM BulletKit; Lonza) was used. Cells from passages 3 to 8 were seeded on 35-mm glass-bottom petri dishes 48 h prior to the experiments and were used after reaching confluence. For immunofluorescence experiments, cells were cultured on 10-mm glass coverslips. In order to stimulate vWF expression, cells were treated for 30 min with 5  $\mu$ M calcium ionophore A23187 (Sigma-Aldrich).

**Immunofluorescence microscopy.** For visualization of vWF in the ECM, cells were fixed with 4% paraformaldehyde in PBS for 10 min and permeabilized at room temperature with 0.1% Triton X-100 (Sigma-Aldrich). To prevent nonspecific antibody binding, endothelial cells were pretreated with 10% bovine serum albumin (Sigma) at room temperature for 60 min and then incubated overnight at 4°C with mouse anti-vWF antibody (MA5-14029; Thermo Fisher Scientific). After being washed with PBS, a secondary goat anti-mouse Alexa Fluor 647 antibody (Abcam) was added for 60 min. Furthermore, all samples were stained with DAPI (4',6'-diamidino-2-phenylindole) to facilitate the identification of the correct focal plane. Finally, coverslips were mounted in mounting medium (Dako, Germany). Fluorescent images were acquired using a Zeiss LSM 710 confocal laser scanning microscope, equipped with a 63 $\times$  NA1.4 HC PL APO CS2 oil immersion objective. The fluorophores were excited at 561 or 405 nm,

respectively. Sequential scanning was applied to avoid concurrent fluorescence signals from two fluorophores.

For the bacterial adhesion assay, confluent HUVECs, being in culture for at least 48 h, were coincubated with *S. aureus* bacterial cells in stationary phase (50  $\mu$ l of a diluted cell suspension per 1 ml of medium), pretreated with LIVE/DEAD BacLight bacterial viability kit (Thermo Fisher Scientific) for 15 min at room temperature. After intensive washing of the sample, three-dimensional analysis using a Zeiss LSM 710 confocal laser scanning microscope was performed. The fluorophores were excited at 488 nm.

**Bacterial adherence to vWF-coated microtiter wells.** Microtiter wells were coated overnight at 4°C with 1  $\mu$ g/well human vWF in 0.1 M sodium carbonate (pH 9.5). The plates were washed with PBS containing 0.5% (vol/vol) Tween 20 (PBST). To block additional protein-binding sites, the wells were treated for 1 h at 22°C with 2% (vol/vol) bovine serum albumin (BSA) in PBS. To test the effect of soluble protein A, the assay was performed in the presence of 2  $\mu$ g recombinant SpA (Thermo Fisher Scientific). The wells were then incubated for 1 h at 37°C with  $1 \times 10^8$  cells of the *S. aureus* Newman strain or its  $\Delta$ spa mutant. After being washed with PBS, adhering cells were fixed with 2.5% formaldehyde for 30 min and stained with 1% crystal violet for 1 min. Following further washing, 100 ml of 10% acetic acid was added, and absorbance at 595 nm was recorded using an enzyme-linked immunosorbent assay (ELISA) plate reader (Bio-Rad).

**Quantification of vWF release by ELISA.** HUVEC monolayers were incubated with the calcium ionophore A23187 for 10 min. The wells were washed three times with PBS and then fixed with 4% paraformaldehyde for 10 min at 4°C. Wells were rinsed with PBS, blocked with 2% BSA in PBS for 1 h at 22°C, and incubated with 1:1,000-diluted rabbit anti-vWF polyclonal antibodies for 1 h at 22°C. The plates were washed and then incubated for 1 h with horseradish peroxidase (HRP)-conjugated goat anti-rabbit IgG diluted 1:1,000. After further washing, *o*-phenylenediamine dihydrochloride was added, and the absorbance at 490 nm was determined using an ELISA plate reader.

**Endothelial cell adhesion assays.** Confluent monolayers of HUVECs were washed three times with PBS to remove antibiotics and treated or not for 10 min with 1  $\mu$ M calcium ionophore A23187. Cell monolayers were then washed 3 times with PBS and incubated with  $10^7$  bacterial cells for 1 h at 37°C. To determine the total number of associated CFU (adherent and internalized), each well was washed 3 times with PBS and cells were lysed by the addition of 0.1% Triton X-100 solution. Bacterial CFU were counted the day after by serial dilution of endothelial cell lysates and plating onto tryptic soy agar (TSA) plates.

**Bacterial adhesion to vWF-coated surfaces.** Adhesion of Newman and Newman  $\Delta$ spa bacteria was assessed on vWF-functionalized surfaces under static and dynamic conditions. For static experiments, bacterial suspensions in PBS were incubated with vWF surfaces for 2 h at 37°C, gently rinsed with PBS, and imaged using an optical microscope Zeiss Axio Observer Z1 and a Hamamatsu camera C10600. For flow experiments, bacterial suspensions were flowed over vWF surfaces during 3 min using a fluidic chamber (39), using a peristaltic pump (Miniplus, Gilson). Two different flow rates were tested (2 and 20 ml min<sup>-1</sup>), corresponding to shear rates of 12 and 120 s<sup>-1</sup>, respectively. Loosely attached bacteria were removed by flowing PBS during 3 min using the corresponding flow rate. Adhering bacteria were imaged using an inverted microscope (Leica DM16000) and counted using the Image J image analysis software (NIH Image).

**Functionalization of substrates and cantilevers with vWF.** Gold-coated glass coverslips and cantilevers (OMCL-TR4, Olympus Ltd., Tokyo, Japan; nominal spring constant,  $\sim 0.02$  N m<sup>-1</sup>) were immersed overnight in an ethanol solution containing 1 mM 10% 16-mercaptododecahexanoic acid-90% 1-mercapto-1-undecanol (Sigma), rinsed with ethanol, and dried with N<sub>2</sub>. Substrates and cantilevers were then immersed for 30 min into a solution containing 10 mg ml<sup>-1</sup> *N*-hydroxysuccinimide (NHS) and 25 mg ml<sup>-1</sup> 1-ethyl-3-(3-dimethylaminopropyl)-carbodiimide (EDC [Sigma]), rinsed with Ultrapure water (ELGA LabWater), incubated with 0.1 mg ml<sup>-1</sup> vWF (Merck) for 1 h, rinsed further with PBS buffer, and then immediately used without dewetting.

**Single-cell force spectroscopy on endothelial cells.** Colloidal probes were obtained by attaching single silica microspheres (6.1- $\mu$ m diameter; Bangs Laboratories) with a thin layer of UV-curable glue (NOA 63, Norland Edmund Optics) to triangular shaped tip-less cantilevers (NP-O10; Bruker) using a Nanowizard III atomic force microscope (JPK Instrument, Berlin, Germany). Cantilevers were then immersed for 1 h in Tris-buffered saline (TBS; Tris, 50 mM; NaCl, 150 mM; pH 8.5) containing 4 mg ml<sup>-1</sup> dopamine hydrochloride (Sigma-Aldrich), rinsed in TBS, and used directly for cell probe preparation. The nominal spring constant of the colloidal probe was determined by the thermal noise method. Then, 50  $\mu$ l of a diluted cell suspension was deposited into the petri dish containing HUVECs at a distinct location within the petri dish; 1 ml of HEPES buffer (HEPES, 10 mM; glucose, 5 mM; MgCl<sub>2</sub>, 1 mM; KCl, 5 mM; NaCl, 140 mM; pH 7.4) was added to the system. The colloidal probe was put in contact with a single bacterial cell and retracted to attach it on the silica microsphere; proper attachment of the cell on the colloidal probe was checked using optical microscopy. Cell probes were used to measure interaction forces on HUVECs at room temperature, and adhesion maps were obtained by recording 8-by-8 or 16-by-16 force-distance curves on 1- by 1- $\mu$ m lamellipodia areas of the cells, using an applied force of 250 pN, a constant approach-retraction speed of 1,000 nm s<sup>-1</sup> (for the Nanowizard III AFM system), and a contact time of 250 ms. Data were analyzed using the Data Processing software from JPK Instruments (Berlin, Germany). Adhesion force and rupture distance histograms were obtained by calculating the maximum adhesion force and the rupture distance of the last peak for each curve.

**Single-cell force spectroscopy on vWF surfaces.** Colloidal probes were prepared as described above, using a Nanoscope VIII multimode atomic force microscope (Bruker Corporation, Santa Barbara,

CA). The nominal spring constants of the colloidal probe cantilevers were determined by the thermal noise method. For cell probe preparation, 50  $\mu\text{l}$  of a suspension of ca.  $1 \times 10^6$  cells was transferred into a glass petri dish containing vWF-coated substrates in PBS. The colloidal probe was brought into contact with a bacterium. Single bacteria were attached on the center of the colloidal probes using a Nanowizard III atomic force microscope (JPK Instruments). The cell probe was then positioned over the vWF substrate without dewetting. Cell probes were used to measure interaction forces on vWF surfaces at room temperature by recording multiple force curves (16 by 16) on different spots using a contact time of 250 ms, a maximum applied force of 250 pN, and approach and retraction speeds of  $1,000 \text{ nm s}^{-1}$ . Adhesion force and rupture distance histograms were obtained by calculating the maximum adhesion force and the rupture distance of the last peak for each curve.

**Single-molecule force spectroscopy on living bacteria.** Bacteria were immobilized by mechanical trapping in porous polycarbonate membranes (Millipore, Billerica, MA) with a pore size similar to the cell size (for details, see reference 40). After filtration of a cell suspension was performed, the filter was gently rinsed with PBS, carefully cut into sections (1 cm by 1 cm), and attached to a steel sample puck using a small piece of double-sided adhesive tape, and the mounted sample was transferred into the AFM liquid cell while avoiding dewetting. Analyses were performed on live bacteria at room temperature ( $20^\circ\text{C}$ ) in PBS using a Nanoscope VIII multimode atomic force microscope (Bruker Corporation, Santa Barbara, CA) and gold-coated cantilevers (Olympus OTR4 with a  $k$  value of  $\sim 0.02 \text{ N m}^{-1}$ ). The spring constants of the cantilevers were measured using the thermal noise method. Arrays of 32-by-32 force curves were recorded on 500- by 500-nm areas using a contact time of 250 ms, a maximum applied force of 250 pN, and approach and retraction speeds of  $1,000 \text{ nm s}^{-1}$ . For loading rate experiments, arrays of 32-by-32 force curves were recorded on 500- by 500-nm areas at increasing retraction speeds: 0.5, 1, 5 and  $10 \mu\text{m s}^{-1}$ . Adhesion and rupture length histograms were generated by considering, for every force curve, the maximum adhesion force and the rupture distance of the last peak. For loading rate experiments, all adhesion peaks were analyzed to take into account all possible interactions. Data were analyzed using the Nanoscope Analysis software from Bruker (Santa Barbara, CA, USA).

## SUPPLEMENTAL MATERIAL

Supplemental material for this article may be found at <https://doi.org/10.1128/mBio.00555-19>.

**FIG S1**, DOCX file, 1.6 MB.

**FIG S2**, DOCX file, 0.9 MB.

**FIG S3**, DOCX file, 0.4 MB.

**TABLE S1**, DOCX file, 0.1 MB.

## ACKNOWLEDGMENTS

Work at the Université Catholique de Louvain was supported by the European Research Council (ERC) under the European Union's Horizon 2020 Research and Innovation Program (grant agreement no. 693630), the FNRS-WELBIO (grant no. WELBIO-CR-2015A-05), the National Fund for Scientific Research (FNRS), and the Research Department of the Communauté Française de Belgique (Concerted Research Action). Funding by the Fondazione CARIPLO (grant Vaccines 2009-3546) to P.S. is acknowledged. Y.F.D. is Research Director at the FNRS.

We thank Jakub Kwiecinski, Joan Geoghegan, and Timothy Foster for fruitful discussion and for providing bacterial strains.

F.V., V.P., A.L., J.M., P.S., G.P., and Y.F.D. designed the experiments, analyzed the data, and wrote the article. F.V., V.P., and A.L. collected the data.

## REFERENCES

- Moreillon P, Que Y-A. 2004. Infective endocarditis. *Lancet* 363:139–149. [https://doi.org/10.1016/S0140-6736\(03\)15266-X](https://doi.org/10.1016/S0140-6736(03)15266-X).
- Fowler VG, Jr, Miro JM, Hoen B, Cabell CH, Abrutyn E, Rubinstein E, Corey GR, Spelman D, Bradley SF, Barsic B, Pappas PA, Anstrom KJ, Wray D, Fortes CQ, Anguera I, Athan E, Jones P, van der Meer JTM, Elliott TSJ, Levine DP, Bayer AS, ICE Investigators. 2005. *Staphylococcus aureus* endocarditis: a consequence of medical progress. *JAMA* 293:3012–3021. <https://doi.org/10.1001/jama.293.24.3012>.
- Pappelbaum KI, Gorzelanny C, Grässle S, Suckau J, Laschke MW, Bischoff M, Bauer C, Schorpp-Kistner M, Weidenmaier C, Schneppenheim R, Obser T, Sinha B, Schneider SW. 2013. Ultra-large von Willebrand factor fibers mediate luminal *Staphylococcus aureus* adhesion to an intact endothelial cell layer under shear stress. *Circulation* 128:50–59. <https://doi.org/10.1161/CIRCULATIONAHA.113.002008>.
- Claes J, Vanassche T, Peetermans M, Liesenborghs L, Vandenbrielle C, Vanhoorelbeke K, Missiakas D, Schneewind O, Hoylaerts MF, Heying R, Verhamme P. 2014. Adhesion of *Staphylococcus aureus* to the vessel wall under flow is mediated by von Willebrand factor-binding protein. *Blood* 124:1669–1676. <https://doi.org/10.1182/blood-2014-02-558890>.
- Claes J, Liesenborghs L, Peetermans M, Veloso TR, Missiakas D, Schneewind O, Mancini S, Entenza JM, Hoylaerts MF, Heying R, Verhamme P, Vanassche T. 2017. Clumping factor A, von Willebrand factor-binding protein and von Willebrand factor anchor *Staphylococcus aureus* to the vessel wall. *J Thromb Haemost* 15:1009–1019. <https://doi.org/10.1111/jth.13653>.
- Dong J-F, Moake JL, Nolasco L, Bernardo A, Arceneaux W, Shrimpton CN, Schade AJ, McIntire LV, Fujikawa K, López JA. 2002. ADAMTS-13 rapidly cleaves newly secreted ultralarge von Willebrand factor multimers on the endothelial surface under flowing conditions. *Blood* 100:4033–4039. <https://doi.org/10.1182/blood-2002-05-1401>.

7. Herrmann M, Hartleib J, Kehrel B, Montgomery RR, Sixma JJ, Peters G. 1997. Interaction of von Willebrand factor with *Staphylococcus aureus*. *J Infect Dis* 176:984–991. <https://doi.org/10.1086/516502>.
8. Hartleib J, Köhler N, Dickinson RB, Chhatwal GS, Sixma JJ, Hartford OM, Foster TJ, Peters G, Kehrel BE, Herrmann M. 2000. Protein A is the von Willebrand factor binding protein on *Staphylococcus aureus*. *Blood* 96: 2149–2156.
9. Bjerketorp J, Jacobsson K, Frykberg L. 2004. The von Willebrand factor-binding protein (vWbp) of *Staphylococcus aureus* is a coagulase. *FEMS Microbiol Lett* 234:309–314. <https://doi.org/10.1111/j.1574-6968.2004.tb09549.x>.
10. Gómez MI, Lee A, Reddy B, Muir A, Soong G, Pitt A, Cheung A, Prince A. 2004. *Staphylococcus aureus* protein A induces airway epithelial inflammatory responses by activating TNFR1. *Nat Med* 10:842. <https://doi.org/10.1038/nm1079>.
11. Gómez MI, Seaghdha MO, Prince AS. 2007. *Staphylococcus aureus* protein A activates TACE through EGFR-dependent signaling. *EMBO J* 26: 701–709. <https://doi.org/10.1038/sj.emboj.7601554>.
12. O'seaghdha M, van Schooten CJ, Kerrigan SW, Emsley J, Silverman GJ, Cox D, Lenting PJ, Foster TJ. 2006. *Staphylococcus aureus* protein A binding to von Willebrand factor A1 domain is mediated by conserved IgG binding regions. *FEBS J* 273:4831–4841. <https://doi.org/10.1111/j.1742-4658.2006.05482.x>.
13. Claes J, Ditkowski B, Liesenborghs L, Veloso TR, Entenza JM, Moreillon P, Vanassche T, Verhamme P, Hoylaerts MF, Heying R. 2018. Assessment of the dual role of clumping factor A in *S. aureus* adhesion to endothelium in absence and presence of plasma. *Thromb Haemost* 118:1230–1241. <https://doi.org/10.1055/s-0038-1660435>.
14. Xiao J, Dufrene YF. 2016. Optical and force nanoscopy in microbiology. *Nat Microbiol* 1:16186. <https://doi.org/10.1038/nmicrobiol.2016.186>.
15. Herbert S, Ziebandt A-K, Ohlsen K, Schäfer T, Hecker M, Albrecht D, Novick R, Götz F. 2010. Repair of global regulators in *Staphylococcus aureus* 8325 and comparative analysis with other clinical isolates. *Infect Immun* 78:2877–2889. <https://doi.org/10.1128/IAI.00088-10>.
16. Ythier M, Resch G, Waridel P, Panchaud A, Gfeller A, Majcherczyk P, Quadroni M, Moreillon P. 2012. Proteomic and transcriptomic profiling of *Staphylococcus aureus* surface LPXTG-proteins: correlation with agr genotypes and adherence phenotypes. *Mol Cell* 111:1123–1139. <https://doi.org/10.1074/mcp.M111.014191>.
17. Hoppenbrouwers T, Sultan AR, Abraham TE, Lemmens-den Toom NA, Hansenová Maňásková S, van Cappellen WA, Houtsmuller AB, van Wamel WJ, de Maat MP, van Neck JW. 2018. Staphylococcal protein A is a key factor in neutrophil extracellular traps formation. *Front Immunol* 9:165. <https://doi.org/10.3389/fimmu.2018.00165>.
18. Sporn LA, Marder VJ, Wagner DD. 1987. von Willebrand factor released from Weibel-Palade bodies binds more avidly to extracellular matrix than that secreted constitutively. *Blood* 69:1531–1534.
19. Uhlen M, Guss B, Nilsson B, Gatenbeck S, Philipson L, Lindberg M. 1984. Complete sequence of the staphylococcal gene encoding protein A. A gene evolved through multiple duplications. *J Biol Chem* 259: 1695–1702.
20. Herman-Bausier P, Labate C, Towell AM, Derclaye S, Geoghegan JA, Dufrene YF. 2018. *Staphylococcus aureus* clumping factor A is a force-sensitive molecular switch that activates bacterial adhesion. *Proc Natl Acad Sci U S A* 115:5564–5569. <https://doi.org/10.1073/pnas.1718104115>.
21. Vitry P, Valotteau C, Feuillie C, Bernard S, Alsteens D, Geoghegan JA, Dufrene YF. 2017. Force-induced strengthening of the interaction between *Staphylococcus aureus* clumping factor B and loricrin. *mBio* 8:e01748-17. <https://doi.org/10.1128/mBio.01748-17>.
22. Sokurenko EV, Vogel V, Thomas WE. 2008. Catch-bond mechanism of force-enhanced adhesion: counterintuitive, elusive, but . . . widespread? *Cell Host Microbe* 4:314–323. <https://doi.org/10.1016/j.chom.2008.09.005>.
23. Kroll MH, Hellums JD, McIntire L, Schafer A, Moake J. 1996. Platelets and shear stress. *Blood* 88:1525–1541.
24. Pawar P, Shin PK, Mousa SA, Ross JM, Konstantopoulos K. 2004. Fluid shear regulates the kinetics and receptor specificity of *Staphylococcus aureus* binding to activated platelets. *J Immunol* 173:1258–1265. <https://doi.org/10.4049/jimmunol.173.2.1258>.
25. Mascari LM, Ross JM. 2003. Quantification of staphylococcal-collagen binding interactions in whole blood by use of a confocal microscopy shear-adhesion assay. *J Infect Dis* 188:98–107. <https://doi.org/10.1086/375826>.
26. Foster TJ, Geoghegan JA, Ganesh VK, Höök M. 2014. Adhesion, invasion and evasion: the many functions of the surface proteins of *Staphylococcus aureus*. *Nat Rev Microbiol* 12:49–62. <https://doi.org/10.1038/nrmicro3161>.
27. Ponnuraj K, Bowden MG, Davis S, Gurusiddappa S, Moore D, Choe D, Xu Y, Hook M, Narayana SV. 2003. A “dock, lock, and latch” structural model for a staphylococcal adhesin binding to fibrinogen. *Cell* 115:217–228. [https://doi.org/10.1016/S0092-8674\(03\)00809-2](https://doi.org/10.1016/S0092-8674(03)00809-2).
28. Herman P, El-Kirat-Chatel S, Beaussart A, Geoghegan JA, Foster TJ, Dufrene YF. 2014. The binding force of the staphylococcal adhesin SdrG is remarkably strong. *Mol Microbiol* 93:356–368. <https://doi.org/10.1111/mmi.12663>.
29. Milles LF, Schulten K, Gaub HE, Bernardi RC. 2018. Molecular mechanism of extreme mechanostability in a pathogen adhesin. *Science* 359: 1527–1533. <https://doi.org/10.1126/science.aar2094>.
30. Herman-Bausier P, Dufrene YF. 2018. Force matters in hospital-acquired infections. *Science* 359:1464–1465. <https://doi.org/10.1126/science.aat3764>.
31. Löf A, Müller JP, Benoit M, Brehm MA. 2017. Biophysical approaches promote advances in the understanding of von Willebrand factor processing and function. *Adv Biol Regul* 63:81–91. <https://doi.org/10.1016/j.jbior.2016.09.010>.
32. Schneider SW, Nuschele S, Wixforth A, Gorzelanny C, Alexander-Katz A, Netz RR, Schneider MF. 2007. Shear-induced unfolding triggers adhesion of von Willebrand factor fibers. *Proc Natl Acad Sci U S A* 104:7899–7903. <https://doi.org/10.1073/pnas.0608422104>.
33. Yakovenko O, Sharma S, Forero M, Tchesnokova V, Aprikian P, Kidd B, Mach A, Vogel V, Sokurenko E, Thomas WE. 2008. FimH forms catch bonds that are enhanced by mechanical force due to allosteric regulation. *J Biol Chem* 283:11596–11605. <https://doi.org/10.1074/jbc.M707815200>.
34. Deis LN, Pemble CW, IV, Qi Y, Hagarman A, Richardson DC, Richardson JS, Oas TG. 2014. Multiscale conformational heterogeneity in staphylococcal protein A: possible determinant of functional plasticity. *Structure* 22: 1467–1477. <https://doi.org/10.1016/j.str.2014.08.014>.
35. Deis LN, Wu Q, Wang Y, Qi Y, Daniels KG, Zhou P, Oas TG. 2015. Suppression of conformational heterogeneity at a protein-protein interface. *Proc Natl Acad Sci U S A* 112:9028–9033. <https://doi.org/10.1073/pnas.1424724112>.
36. Smith EJ, Visai L, Kerrigan SW, Speziale P, Foster TJ. 2011. The Sbi protein: a multifunctional immune evasion factor of *Staphylococcus aureus*. *Infect Immun* 79:3801–3809. <https://doi.org/10.1128/IAI.05075-11>.
37. Boles BR, Thoendel M, Roth AJ, Horswill AR. 2010. Identification of genes involved in polysaccharide-independent *Staphylococcus aureus* biofilm formation. *PLoS One* 5:e10146. <https://doi.org/10.1371/journal.pone.0010146>.
38. O'Halloran DP, Wynne K, Geoghegan JA. 2015. Protein A is released into the *Staphylococcus aureus* culture supernatant with an unprocessed sorting signal. *Infect Immun* 83:1598–1609. <https://doi.org/10.1128/IAI.03122-14>.
39. Vanzieleghem T, Couniot N, Herman-Bausier P, Flandre D, Dufrene YF, Mahillon J. 2016. Role of ionic strength in staphylococcal cell aggregation. *Langmuir* 32:7277–7283. <https://doi.org/10.1021/acs.langmuir.6b00499>.
40. Dufrene YF. 2008. Atomic force microscopy and chemical force microscopy of microbial cells. *Nat Protoc* 3:1132. <https://doi.org/10.1038/nprot.2008.101>.